Monthly Notices
of the
ROYAL ASTRONOMICAL SOCIETY

Mon. Not. R. Astron. Soc. **419,** 2912–2920 (2012) doi:10.1111/j.1365-2966.2011.19933.x

The recondite★ intricacies of Zeeman Doppler mapping

M. J. Stift,[1] F. Leone[2] and C. R. Cowley[3]†

[1]*Institut für Astronomie (IfA), Universität Wien, Türkenschanzstrasse 17, A-1180 Wien, Austria*
[2]*Dipartimento di Fisica e Astronomia, Università die Catania, Sezione Astrofisica, Via S. Sofia 78, I-95123 Catania, Italy*
[3]*Department of Astronomy, University of Michigan, Ann Arbor, MI 48109-1042, USA*

Accepted 2011 September 30. Received 2011 September 12; in original form 2011 June 14

ABSTRACT

We present a detailed analysis of the reliability of abundance and magnetic maps of Ap stars obtained by Zeeman Doppler mapping (ZDM). It is shown how they can be adversely affected by the assumption of a mean stellar atmosphere instead of appropriate 'local' atmospheres corresponding to the actual abundances in a given region. The essence of the difficulties was already shown by Chandrasekhar's picket-fence model. The results obtained with a suite of Stokes codes written in the ADA programming language and based on modern line-blanketed atmospheres are described in detail. We demonstrate that the high metallicity values claimed to have been found in chemically inhomogeneous (horizontally and vertically) Ap star atmospheres would lead to local temperature structures, continuum and line intensities, and line shapes that differ significantly from those predicted by a mean stellar atmosphere. Unfortunately, past applications of ZDM have consistently overlooked the intricate aspects of metallicity with their all-pervading effects. The erroneous assumption of a mean atmosphere for a spotted star can lead to phase-dependent errors of uncomfortably large proportions at varying wavelengths both in the Stokes I and V profiles, making precise mapping of abundances and magnetic field vectors largely impossible. The relation between core and wings of the Hβ line changes, too, with possible repercussions on the determination of gravity and effective temperature. Finally, a ZDM analysis of the synthetic Stokes spectra of a spotted star reveals the disturbing differences between the respective abundance maps based on a mean atmosphere on the one hand, and on appropriate 'local' atmospheres on the other. We then discuss what this all means for published ZDM results. Our discussion makes it clear that realistic local atmospheres must be used, especially if credible small-scale structures are to be obtained.

Key words: line: profiles – techniques: spectroscopic – stars: atmospheres – stars: chemically peculiar – stars: magnetic field – starspots.

1 INTRODUCTION

Zeeman Doppler mapping (ZDM) has made considerable progress over recent years, thanks mainly to powerful new spectrographs which yield high signal-to-noise ratio (S/N) polarized spectra in all four Stokes $IQUV$ parameters. Whereas in the early days of Doppler mapping, intensity spectra only were used to derive abundance maps (see e.g. Rice, Wehlau & Khokhlova 1989), the addition of spectra in circular polarization (Stokes V) soon opened up the possibility to simultaneously determine both the magnetic field structure and the abundance distributions of various chemical elements. However, right in the first days of ZDM, Brown et al. (1991) gave a caveat: linear polarization data (Stokes Q and U) would be needed to derive reliable magnetic maps for Ap stars. Still, even into the new millennium, Doppler maps of magnetic stars have been published, based on Stokes I and V only (Kochukhov et al. 2002; Lüftinger et al. 2010), although instruments capable of determining accurate Q and U profiles have by now been developed. Numerous Doppler maps of magnetic stars even rely solely on Stokes I (Kuschnig et al. 1998; Lüftinger, Kuschnig & Weiss 1998; Piskunov et al. 1998; Lüftinger et al. 2003). The reader of the articles cited will surely note that elemental overabundances resulting from Doppler imaging frequently appear quite unrealistic. Consider for example the results for ι Cas where according to Kuschnig et al. (1998) in parts of the atmosphere, $\log(N_{\rm Cr}/N_{\rm tot}) = -1.50$. Similarly, for κ Psc, Piskunov et al. (1998) find that over a considerable part of the surface, $\log(N_{\rm Fe}/N_{\rm tot}) = -1.81$, while Cr, according to their fig. 1, varies between -6.09 and 0.27! For comparison, the solar abundance is -5.6 (Asplund et al. 2009). The question arises not only how a star can possibly contain more chromium than hydrogen in parts of its atmosphere,

★Recondite: dealing with very profound, difficult or abstruse subject matter; requiring special knowledge to be understood (http://dictionary.reference.com/browse/recondite).

†E-mail: cowley@umich.edu

but also how such an enormous overabundance could build up and whether such an atmosphere could ever remain stable. Note that the modelling of equilibrium stratifications in Ap stars (Alecian & Stift 2007; LeBlanc et al. 2009) has not so far yielded a single case with such extreme iron or chromium abundances. Could these excessive values not rather be due to serious shortcomings in the ZDM procedure?

Fortunately, high-quality Stokes *QU* profiles have now become available, and this might be thought to ensure uniqueness of the magnetic and abundance maps. Based on recently obtained Stokes *IQUV* profiles, a major revision both of the previously published magnetic geometry and of the elemental abundance distributions of the famous Ap star α^2 CVn has taken place. The new maps appear to validate the analysis of Brown et al. (1991). Whereas the Stokes *I* and *V* based analysis by Kochukhov et al. (2002, hereafter K02) yielded a minimum field of -6.5 kG and a maximum field of $+5.1$ kG, these values have now become -3.5 and $+3.5$ kG, respectively (Kochukhov & Wade 2010, hereafter K10); we also see substantial changes in the structure both of the meridional and the azimuthal field. The respective field distributions from K02 and K10 at phases 0.20 and 0.40 are strikingly different, and it is quite surprising to see that a sharp maximum in field strength is accompanied by an almost horizontal inclination of the magnetic field.

The K10 iron maps bear little resemblance to the K02 maps, and there are a few noticeable differences in the chromium maps; there is no obvious correlation between field direction or strength and the abundance features. A 2.3-dex amplitude in the Fe abundances has increased to a staggering 4.9 dex, a fact that cannot be explained by magnetic intensification (see Stift & Leone 2003). However, there are not only these differences between the old and the new maps that are distressing, but there is also the question of (optimum) regularization. In an ill-posed problem such as ZDM, regularization is necessary to obtain meaningful and hopefully unique maps of elemental abundances and of the magnetic field vector; these maps should combine minimum structure (complexity) with a good fit to the observed Stokes *IQUV* profiles. In the past, maximum entropy regularization has been used extensively (see e.g. Vogt, Penrod & Hatzes 1987), but nowadays it is largely replaced by Tikhonov regularization which minimizes the sum of the squared differences between the unknowns (abundances, magnetic field components) of any combination of two surface elements (see equation 5 of K10). Please keep in mind that both Tikhonov and maximum entropy regularizations are purely mathematical constraints which do not necessarily reflect the physical reality: radiatively driven diffusion in magnetic stellar atmospheres might not lead to smooth but rather to patchy surface structure (Alecian & Stift 2010).

Even with all four Stokes parameters used by K10, the magnetic geometry depends in a sensitive way and to an uncanny degree on the value of the regularization parameter. Obviously, the smaller the latter gets, the more fine structure in the magnetic field appears, but in addition, changes in the regularization parameter make field maxima not only change appreciably in value but these maxima also appear to travel over substantial distances to new locations (compare figs 6 and 8 in K10). In that context, the reader of the K10 paper, having access to abundance maps for only two values of the regularization parameter, is certainly entitled to ask himself whether this travel proceeds smoothly or rather in erratic jumps. The reader will also note that Stokes *Q* and *U* data for a mere three or four out of 20 phases are mainly responsible for the complete revision of the surface abundance and field strength maps (this will be discussed in Section 7), while there are still a lot of profiles that have not been fitted to within the estimated observational errors.

Apparently, the method used by K10 is not robust, since the results depend too strongly on the value of the regularization parameter. As K10 have shown themselves in their figs 6 and 8, the value of the regularization parameter not only determines the resolution of the maps – as one would ideally expect – but to an uncomfortable degree also their large-scale structure. Is this fact due to some numerical instability and/or to weird behaviour of the Tikhonov regularization, or is it rather indicative of something even more disturbing, i.e. do we have to admit that the input physics used so far by K10 are seriously inadequate? Could it be that the ZDM code yields a beautiful but incorrect and unphysical solution that also depends on erroneous assumptions as to, for example, the atmospheric structure? This is what we will explore in the following sections.

2 THE TOOLS

Any thorough investigation of ZDM and its input physics requires a set of powerful numerical codes. One has to be able to calculate highly accurate Stokes profiles for stellar atmospheres permeated by strong magnetic fields of various geometries. There is the need for opacity sampled stellar atmospheres which allow for arbitrary, perhaps even vertically stratified, elemental abundances. The spectra of spotted stars have to be calculated using at least two different atmospheric models (for a single spot), but more flexible and realistic abundance patterns may have to make use of many more model atmospheres, up to 10 and even more. Finally, it is useful to be able to verify how (Zeeman) Doppler maps reflect or fail to reflect any spotted structure adopted in the synthesis of Stokes profiles of magnetic stars.

All but one of the codes used in our investigation are based on COSSAM which stands for 'Codice per la sintesi spettrale nelle atmosfere magnetiche' described herewith. Parts of COSSAM can be traced back to ADRS3 (Chmielewski 1979) which itself is an evolved version of the FORTRAN adaptation by Peytremann et al. (1967) of the ALGOL 60 code ANALYSE 65 by Baschek, Holweger & Traving (1966). COSSAM and all the other codes are written in ADA, an object-oriented language whose syntax derives from the ALGOL family of languages and which is used mainly for safety-critical applications such as flight software but is also eminently suitable for scientific computing. ADA makes it possible to achieve a remarkably high degree of portability, its encapsulated software modules ('packages') allow extensive verbatim software reuse and there are unique language constructs ('tasks') for concurrent processing which can be employed for highly efficient parallel computing with very little synchronization overhead thanks to 'protected types'. Finally, it should be mentioned that free ADA compilers of the same quality as those provided for EADS (makers of Airbus) or Boeing are provided free of charge and are included in every Linux distribution. For more details, see Stift (1998, 2000) Stift & Dubois (1998) and Wade et al. (2001).

COSSAM is a code that calculates full Stokes *IQUV* profiles in local thermodynamic equilibrium (LTE) either for the solar case (at a given point on the solar surface) or for the stellar case (integral over the visible hemisphere). Atomic transition data are usually taken from the Vienna Atomic Line Database (VALD; Piskunov et al. 1995; Kupka et al. 1999), and often include the constants for radiation damping, Stark broadening and van der Waals broadening. When these constants are unavailable, classical radiation

damping and Unsöld van der Waals broadening are taken, together with Stark broadening according to Gonzalez, Artru & Michaud (1995). For the Voigt and Faraday profiles of the metal lines, the complex rational function given by Hui, Armstrong & Wray (1978) is used; the hydrogen line profiles are calculated by means of the approximation found in TLUSTY (Hubeny & Lanz 1995). Zeeman splittings are calculated from the J-values of the lower and upper energy levels, respectively, and their Landé factors; in case these data are lacking, a simple Zeeman triplet is assumed. In order to establish the line absorption matrix in the polarized radiative transfer equation (RTE), full opacity sampling is carried out, separately for the σ_-, σ_+ and π components. The required continuous opacities come from the ATLAS12 (Kurucz 2005) routines translated to ADA (Kurucz 2005; Bischof 2005) and encapsulated in a re-usable multipurpose package. Special care is applied to the treatment of the Lyman, Balmer and Paschen discontinuities according to the level dissolution probability method of Hubeny, Hummer & Lanz (1994). The formal solution to the polarized RTE is carried out using the Zeeman Feautrier method (Auer, Heasley & House 1977; Alecian & Stift 2004) or the Diagonal Element Lambda Operator (DELO) method (Rees, Durrant & Murphy 1989). Spatial integration of the local Stokes profiles over the visible hemisphere can take advantage of an optimum grid due to Stift (1985). Opacity sampling, the most time-consuming part of the code, is entirely and efficiently parallelized and so allows one to take full advantage of the power of modern symmetric multiprocessing (SMP) machines of 1–48 cores and more, all of this without having recourse to MPI or to related software libraries.

COSSAMSPOT is a code derived from COSSAM that calculates full Stokes *IQUV* profiles for stars doted with as many as 10 spots. As we shall show below, atomic transition data have to be accommodated not just for 1 atmosphere but for up to 10 atmospheres (or even more). Thanks to the object orientation of ADA, this can be done in a straightforward way through the use of *generic packages* which constitute *templates* (in the C++ diction) that can be *instantiated* with actual parameters. It thus becomes possible to model e.g. the spectrum of a star with a number of spots, each of which is made up of concentric rings of different abundance and/or temperature. Clearly, spotted stars require a grid that is different from the observer-centred grid used in COSSAM: here we have a corotating grid where the whole surface of the star is split into elements of about equal area (for a typical such grid, see e.g. fig. 1 in Vogt et al. 1987).

For the stellar atmosphere models, we rely on the ATLAS12 code (Kurucz 2005), translated to ADA by Bischof (2005) and offering a restricted number of Kurucz's original options; the code has subsequently been thoroughly debugged by Stift and now offers most of the original options. ATLASADA makes provisions for stratified atmospheres and thanks to the parallelization of the opacity sampling part can provide excellent frequency resolution. Apart from these two improvements and from better defined interfaces to the subprograms, the input physics are identical to those of the official FORTRAN version.

Finally, the Doppler mapping code by Stift (1996) has been completely rewritten and is now based on the latest version of COSSAM. At the time of writing, COSSAMDOPPLER derives abundance maps from Stokes I profiles only; the magnetic field geometry is taken into account but has – for our tests – to be the same as the input geometry to COSSAMSPOT. Maximum entropy regularization is combined with a simple gradient search, ensuring convergence to the desired high-quality fit to the intensity profile within 6–10 iterations in favourable circumstances.

3 THE PICKET-FENCE MODEL AND ATLAS12 STELLAR ATMOSPHERES

The repercussions of line blanketing on the structure of a stellar atmosphere were treated in an analytical way by Chandrasekhar (1935). His so-called picket-fence model is based on the assumptions of a frequency-independent continuum opacity, of lines distributed randomly and uniformly over the spectrum and of a constant opacity ratio between the lines (with square profiles) and the continuum – for a very readable presentation of this method, see Mihalas (1970). Chandrasekhar showed that with increasing line opacity, the temperature gradient increases, and the temperature at the upper boundary of the atmosphere decreases. Later numerical approaches allowed for more realistic spectral line distributions, starting with 30 000 lines for Procyon (Strom & Kurucz 1966) and going up to millions of lines (Kurucz & Bell 1995); they give a very detailed idea of how important line blocking and backwarming can become and how these affect the structure of a stellar atmosphere.

Chandrasekhar's picket-fence model is an astrophysical classic, but nobody seems to have spent much thought on it in the context of ZDM. Therefore, let us investigate what fully line-blanketed atmospheres calculated with ATLAS12 (Kurucz 2005) look like for the extreme abundances, especially of iron, claimed by K10 for α^2 CVn. For this purpose, we have established a grid of models with $T_{\rm eff} = 12\,000$ K, $\log g = 4.0$, and with iron abundances that cover a wide range, namely $A({\rm Fe}) = 6.50$, 7.00, 7.50, 8.00, 8.50, 9.00, 9.50, 10.00, 10.25 and 10.50 (on a scale where the hydrogen abundance is 12.00). For simplicity's sake, we took solar abundances for all the other elements, allowing us to single out the effects of just one parameter. Convergence of the models with large overabundances turned out to be excruciatingly slow at times, and it also proved necessary to proceed in small steps from $A({\rm Fe}) = 9.00$ to 10.00 and beyond in order to obtain any convergence at all. Thanks to the parallelized ADA version of ATLAS12, we could afford satisfactory sampling with 120 000 frequency points. Fig. 1 clearly illustrates

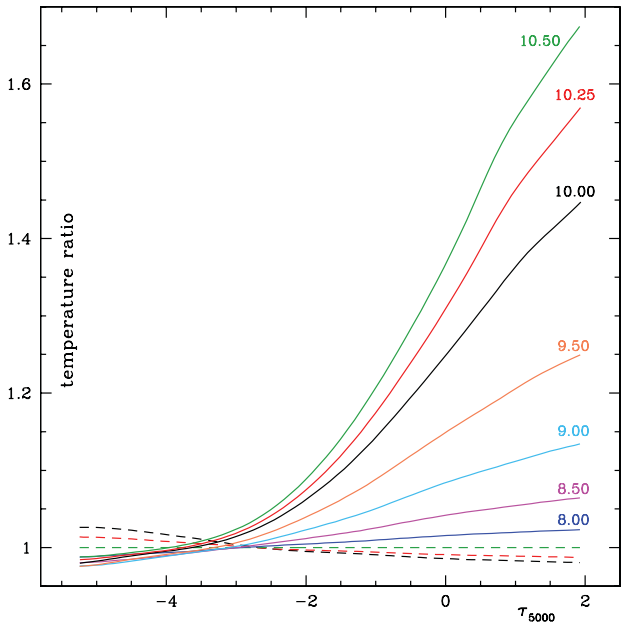

Figure 1. Variations, as a function of iron abundance, in the run of temperature with $\log \tau_{5000}$ in an ATLAS12 model atmosphere with $T_{\rm eff} = 12\,000$ K, $\log g = 4.0$ (all other elements have solar abundances). The curves pertain to iron abundances ranging from $A({\rm Fe}) = 6.50$ to 10.50 and are plotted relative to the temperature profile of the $A({\rm Fe}) = 7.50$ model.

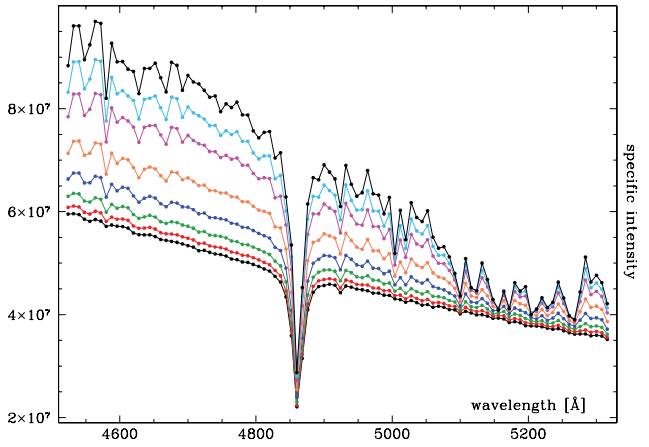

Figure 2. Line-blanketed spectra for ATLAS12 model atmospheres with $T_{\rm eff} = 12\,000$ K, $\log g = 4.0$ and varying iron abundances. For all other elements, solar abundances have been assumed. Means of the specific intensity at the centre of the disc (in erg cm^{-2} s^{-1} Hz^{-1} sr^{-1}) have been calculated over 8-Å intervals. The curves pertain – from bottom to top – to A(Fe) = 7.50, 8.00, 8.50, 9.00, 9.50, 10.00, 10.25 and 10.50.

how the temperature gradient steepens with increasing metallicity, and how at $\log \tau_{5000} = 2.0$, the bottom of the atmosphere gets hotter, whereas the top at $\log \tau_{5000} = -5.3$ becomes cooler, at least up to moderate metallicities. Let us point out that the differences between the curves for A(Fe) = 6.50 and 8.00 are smaller than the differences between the curves for A(Fe) = 10.00 and 10.25! In order to illustrate the vast changes in line blocking between A(Fe) = 7.50 and 10.50 over the interval covered by the metal lines used in K10, we plot in Fig. 2 Stokes I specific intensity means over 8-Å intervals. At these wavelengths, the continuum of the A(Fe) = 10.50 atmosphere lies considerably above the continuum of the A(Fe) = 7.50 atmosphere in order to ensure constant total flux for the given effective temperature in the presence of heavy blanketing. Note the nice depression around 5200 Å which develops for A(Fe) > 10.00 and which is probably related to the well-known feature used to define a peculiarity index (Maitzen 1976). Given the large differences in atmospheric structure, can we expect spectral line shapes to be insensitive to metallicity effects?

4 LINE SHAPES AND SIMPLE ARITHMETICS

Notwithstanding the ground-breaking work of Chandrasekhar (1935), differential line blanketing – between spot and photosphere – in stellar atmospheres has never been taken into account by Doppler mapping experts. Especially for recent work, this seems a bit strange since Khan & Shulyak (2007) have shown the non-negligible effects of Fe and Cr overabundances on stellar atmospheres and on abundance estimates. True, for very small abundance differences over the stellar surface, it is absolutely tolerable to approximate the 'local atmospheres' by an atmosphere corresponding to the mean metallicity (but see below for the definition of 'very small'). However, in the light of the findings of Khan & Shulyak (2007), it is certainly time to challenge this mean atmosphere assumption in those cases when iron abundances attain and exceed A(Fe) = 9.50, and to show that line profiles calculated with the corresponding high-metallicity atmospheres differ significantly from those calculated for example with a A(Fe) = 7.50 atmosphere or even a A(Fe) = 8.50 atmosphere.

For this purpose, Fig. 3 displays, for the λ 4924 iron line (plus actual blending lines) at the centre of the stellar disc, normalized

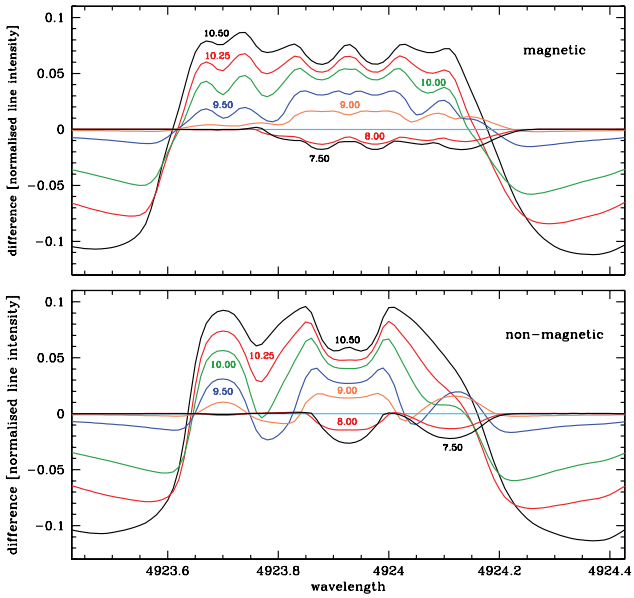

Figure 3. Abundance-dependent, differential shapes of the normalized Stokes I profile of the Fe II line at 4923.927 Å. The plots give, for a number of iron abundances A(Fe), the differences $I^A_{850} - I^A_A$ at the centre of the stellar disc; the subscript denotes the iron abundance assumed in the establishment of the stellar atmosphere later used for the spectral synthesis, the superscript the actual iron abundance adopted. Both the non-magnetic case (lower panel) and the magnetic case (upper panel) with field strength 4400 G and 90° angle between field vector and line of sight are shown. The model atmospheres are the same as presented in Fig. 2.

intensity differences $I^A_{850} - I^A_A$ for various adopted Fe abundances A(Fe). The subscript stands for the iron abundance adopted in the establishment of the stellar atmosphere, the superscript for the actual iron abundance assumed for the spectral synthesis. The abundance grid for this test covered A(Fe) = 7.50, 8.00, 8.50, 9.00, 9.50, 10.00, 10.25 and 10.50. In the lower panel, we plot the non-magnetic intensity differences, in the upper panel the differences for a 4400-G field inclined by 90° with respect to the line of sight. For A(Fe) = 10.00, the differences attain about 5 per cent of the continuum both in the non-magnetic and in the magnetic case, and they get substantially larger (more than 10 per cent) with increasing iron abundance. In view of these results, it is difficult to understand how K10 (in Section 3) can come to the conclusion that *'the local line profiles are sensitive to model structure effects to a much smaller degree than to changes of abundance or magnetic field'*. It also emerges from these plots that for ultrahigh abundances, it becomes more or less impossible to correctly model the line core. The ATLAS12 atmospheres – for good reasons – do not go further outwards than about $\log \tau_{5000} = 5.0\,10^{-6}$ and this turns out to be no longer sufficient for extremely strong lines. While this problem hardly shows up when using a A(Fe) = 8.50 atmosphere, it becomes an object of preoccupation with the correct atmospheric models.

The whole problem with the adoption of a single atmospheric model for the mapping of spotted stars with large differences in abundances over the surface boils down to the inequality

$$(S_1 I_{A1}/C_{A1} + S_2 I_{A2}/C_{A1}) \neq (S_1 I_{A1} + S_2 I_{A2})/(S_1 C_{A1} + S_2 C_{A2}),$$

where I stands for the line intensity, C for the continuum intensity. S_1 and S_2 are the fractions of the visible surface taken by spot and remaining atmosphere, respectively, $A1$ and $A2$ are the

respective abundances inside and outside the spot. The left-hand side corresponds to the approximation used in all previous ZDM work, whereas the right-hand side gives the correct formula for the observed normalized intensity. It comes as no surprise that the consequences of not taking into account the metallicity-dependent line shapes and absolute line intensities can be quite serious as we shall demonstrate further in the following sections.

5 ABUNDANCES AND MAGNETIC FIELD STRENGTHS

What can we learn from the plots given in the section above as far as the determination of abundances is concerned? Extreme Fe abundances in localized spots as claimed by K10 for α^2 CVn – there would be three iron atoms for every 100 hydrogen atoms – seem a bit unrealistic but are no obstacle to modelling with ATLAS12 and with COSSAM. We have calculated the full Stokes parameters of a spotted star with $v \sin i = 18$ km s^{-1}, inclination $i = 60^\circ$, and covered by a large spot of 50° radius at 40° latitude. For the spot, we adopted $A(\mathrm{Fe}) = 10.00$, and for the remaining part of the star, $A(\mathrm{Fe}) = 8.50$. One set of spectra was calculated with a $A(\mathrm{Fe}) = 8.50$ atmosphere throughout, the other set is based on the actual value, $A(\mathrm{Fe}) = 10.00$, inside the spot.

The lower panel of Fig. 4 displays – for five different rotational phases – the differences between the normalized Stokes I spectrum obtained with the same atmosphere all over the star (as done by K02/K10 and henceforth denoted as the 'usual' spectrum) and the correct spectrum. These differences with a maximum of about 7 per cent – which can by no means be considered small or negligible in view of a central line intensity of about 40 per cent of the continuum – change their positions with phase due to the rotation. In a ZDM calculation, based on the 'usual' global atmospheric model, this would translate to appropriately placed spurious overabundances, a problem which we shall discuss later in more detail.

The upper panel of Fig. 4 reveals that polarization is affected too. The tilted and eccentric dipole model adopted leads to respective minimum and maximum field strengths of 1500 and 5500 G. The amount by which Stokes V can be in error reaches some 2 per cent, which has to be put in relation to the maximum signal of about 10 per cent. Again, the differences change position with phase and simulate spurious magnetic field structure.

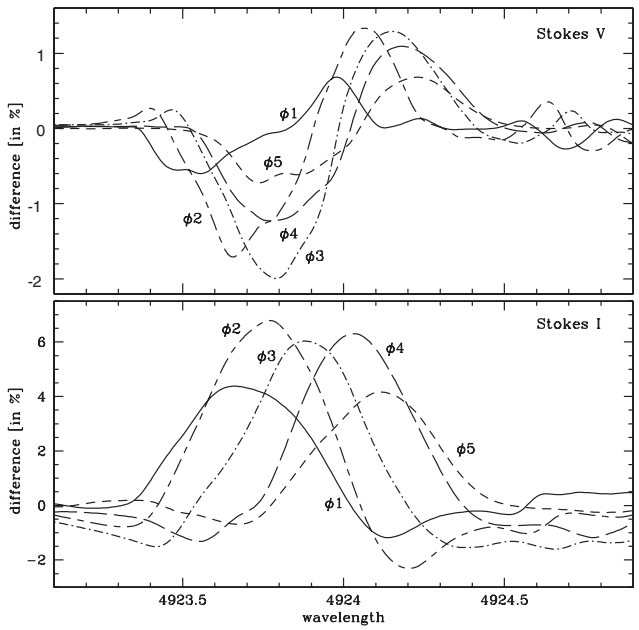

Figure 4. Differences between the Stokes I and V profiles of the Fe II line at 4923.927 Å of a rotating star with a single spot, calculated with the correct (two) model atmospheres for the star and its spot on the one hand, with a mean model for star and spot on the other hand. The plot shows the normalized differences for five phases ($\phi 1 = 0.000$, $\phi 2 = 0.125$, $\phi 3 = 0.250$, $\phi 4 = 0.375$ and $\phi 5 = 0.500$) in the sense 'mean atmosphere' minus 'correct atmosphere'. A spot of 50° radius is situated at a latitude of 40° and displays a 1.5-dex overabundance of iron with respect to the $A(\mathrm{Fe}) = 8.50$ abundance over the rest of the star. The inclination of the star is 60°, the respective magnetic field extrema are 1500 and 5500 G. At $\phi 1$ and $\phi 5$, the spot is near the limb and at $\phi 3$, it is almost centred.

6 THE Hβ LINE

The profile of the Hβ line, together with the profiles of other Balmer lines, are used for the determination of the effective temperature and the surface gravity of a star. If, as shown above, the shapes of iron lines change with the metallicity of the stellar atmosphere, what will happen to the Balmer lines in a spotted star and to the stellar parameters derived from them? We have tried to figure this out at least partially by calculating phase-dependent spectra for a star with eight abundance regions representing six different iron abundances. The results are shown for four phases in Fig. 5, together with the corresponding abundance distributions over the visible stellar hemisphere. The dotted curves correspond to the Hβ line derived with the 'usual' $A(\mathrm{Fe}) = 8.50$ atmosphere – it must remain constant irrespective of phase since we do not consider Zeeman splitting of hydrogen lines – the full lines are based on the six correct model atmospheres.

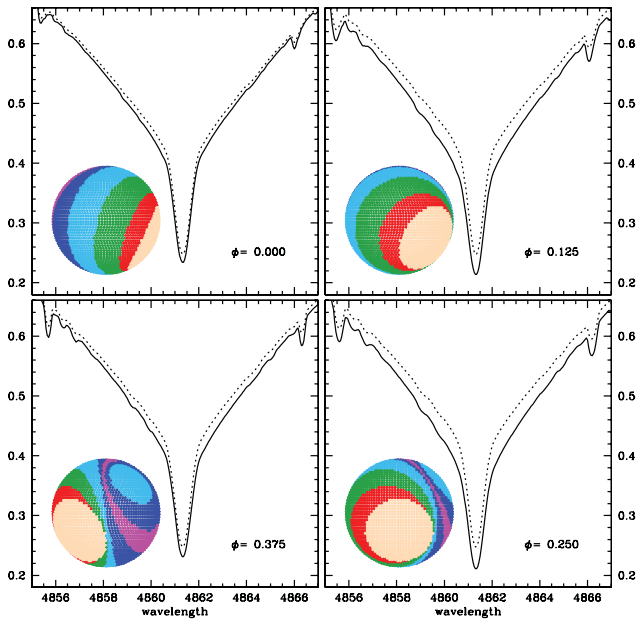

Figure 5. Surface abundance distributions and corresponding Hβ profiles at four different rotational phases of a star with a complex spot structure and six different iron abundances $A(\mathrm{Fe})$, namely 7.50 (magenta), 8.00 (blue), 8.50 (sky blue), 9.00 (green), 9.50 (red) and 10.00 (peach). The star is seen equator-on. The full lines pertain to the normalized Stokes I profiles calculated at the phases indicated with the correct atmospheres corresponding to the adopted abundances, and the dotted lines are based on the 'usual' $A(\mathrm{Fe}) = 8.50$ atmosphere and remain constant.

It is immediately clear that the Hβ line does not remain unaffected by high-metallicity spots, in accord with the findings of Leone & Manfré (1997). In the particular case presented here, the core is deeper by up to 5 per cent of the continuum and the inner wings larger, something that may possibly have repercussions on the determination of stellar parameters. The outer wings turn out to change by less than 1 per cent at wavelengths more than 10 Å distant from the line centre. It remains to be seen if these profile changes are related to the core-wing anomaly discussed by Cowley et al. (2001).

7 THE DETECTABILITY OF MAGNETIC FINE STRUCTURE

K10 claim to have found 'high-contrast surface distributions' of Fe and Cr together with 'small-scale magnetic structures' and a global field dominated by 'high-contrast magnetic spots'. Looking at their fig. 6, we indeed see 'the high-contrast structure of the field strength at smaller spatial scales' consisting in particular of two very intense magnetic spots of surprisingly small extension; at the same time, their fig. 9 does not reveal any similar small-scale structure in the abundance distributions of Fe or Cr. The magnetic spots exhibit diameters which lie in the approximate range of 15°–25°, lines of constant field strength are separated by as little as 8° (for a difference of 0.5 kG) and lines of constant abundances by about 6° (for a difference of 0.5 dex in abundances).

Before embarking on the numerical modelling of the signal of a high-contrast magnetic spot, let us shortly dwell on just two appropriate observational considerations. Looking at fig. 7 in K10, it appears that a feature as small as 20° is resolved which in terms of spherical harmonics would correspond to $m = 18$. However, at the same time, fig. 12 in K10 goes no further than $l = m = 10$, with hardly any power left in this moderately high harmonic. This raises first doubts as to the actual detectability of small-scale structures, doubts which are not dispelled when rotational Doppler shifts are related to the resolution of the MuSiCoS spectrograph on the Pic-du-Midi used by K10. The rather moderate resolution of the spectra, namely $R = 35\,000$, translates to 0.14-Å full width at half-maximum for the iron lines used by K10. If one takes a spot of 20° diameter whose leading edge is exactly on the limb and the trailing edge thus 70° from the line of sight, in terms of Doppler shift the difference in wavelength between leading and trailing edge is a mere 0.018 Å, corresponding to one-eighth of the resolution of the spectrograph.

7.1 The signal of a high-contrast magnetic spot

There can thus be hardly any doubt that the signal of a small-scale magnetic spot – even when the contrast to the surroundings is high – will be exceedingly faint and washed out due to the limited resolution of the spectrograph. The question immediately arises whether such hypothetical spots are observable at all – remember that they tend to appear and to disappear with the regularization parameter – given that any error in the assumed atmospheric model translates to erroneous synthetic Stokes profiles on which abundance and magnetic field estimates are based.

We have for simplicity's sake assumed a centred dipole oblique rotator model with 90° obliquity, seen equator-on, a polar field strength of 4.0 kG and a spot of 20° diameter (indeed a small-scale structure) at 10° latitude. Based on this geometry, we then established two phase-dependent sets of Stokes spectra with an iron abundance of $A(\mathrm{Fe}) = 10.00$ in the spot, and with $A(\mathrm{Fe}) = 8.50$ over the rest of the stellar surface. One set uses, in the 'usual' way, the same atmospheric model outside and inside the spot, with the global field strength distribution given by the oblique rotator model, but multiplied by 1.0, 1.5 and 2.0, respectively, inside the spot. For the second set, we adopted the correct approach, using the appropriate atmospheric models corresponding to the assumed abundances, i.e. a $A(\mathrm{Fe}) = 10.00$ Atlas12 model for the spot, and again calculated models with a 1.0-, 1.5- and 2.0-fold enhancement of the magnetic field inside the spot.

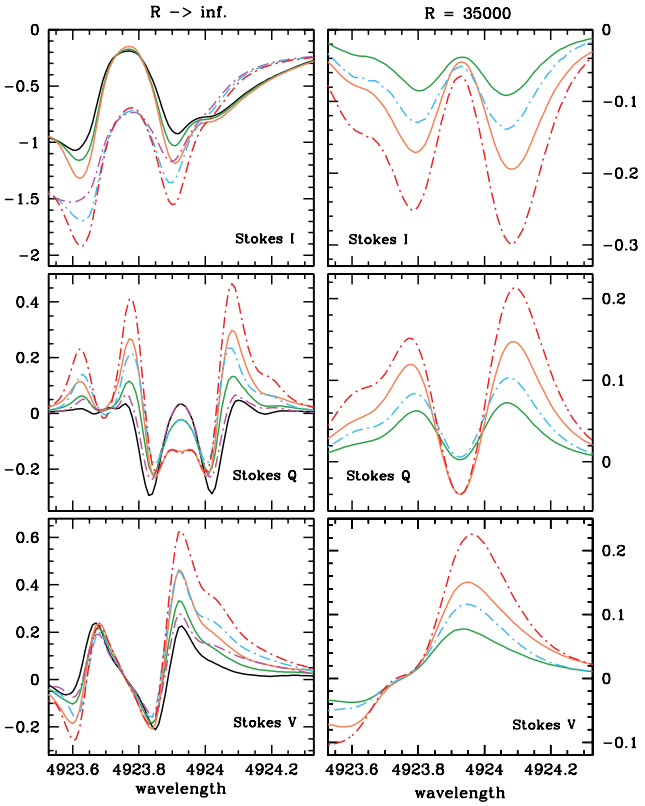

Figure 6. Detectability of magnetic fine structure in a star with a spot of 20° diameter and $A(\mathrm{Fe}) = 10.00$ abundance. Outside the spot, an abundance of $A(\mathrm{Fe}) = 8.50$ is assumed. The full curves pertain to the 'usual' model, the dot–dashed lines to the correct model. The panels to the left display Stokes profiles relative to those of a spotless star, calculated for essentially infinite spectral resolution, and with field strengths inside the spot multiplied by factors of 1.00 (black, magenta), 1.50 (green, sky blue) and 2.00 (peach, red), respectively. Units are per cent of the continuum or per cent polarization. The panels to the right display profiles relative to those of a star with no field enhancement in the spot, convolved to the resolution of the K10 spectra. Note the difference in scale!

In the right-hand panels of Fig. 6, we display differential Stokes I and Q profiles at phase 0.15, differential Stokes V profiles at phase 0.25 (at these phases, the respective signals due to the spot are largest), all of them with a spectral resolution of $R = 35\,000$. The differential signal in Stokes U is much weaker for the adopted geometry than in Q or V, and therefore not plotted. The differences are given in the sense 'field enhanced spot' minus 'normal field spot'. The full lines pertain to the 'usual' model, the dot–dashed lines to the correct model, for an enhancement of 50 per cent (green, sky blue) and 100 per cent (peach, red). ZDM addicts will find the maximum differential signal in Stokes Q from a spot in which the magnetic field is increased from 2 to 3 kG disappointingly low, namely a mere 0.10 per cent for the correct model and barely 0.07

per cent for the 'usual' model. The situation is almost identical in Stokes V. Even a staggering field increase in the spot from 2 to 4 kG is reflected in no more than a 0.22 per cent differential signal in Stokes Q and V and 0.15 per cent for the 'usual' model. Note that these differential signals are not only disturbingly small but that fig. 5 of K10 shows quite a few Q, U and V profiles which are not fitted to that accuracy!

Even at almost infinite resolution – left-hand panels of Fig. 6 – a 50 per cent increase in field strength in the high-abundance spot adds at most 0.22 per cent to the Stokes Q signal and 0.18 per cent to the V signal, taking the correct two atmospheric models. Here, we have plotted the Stokes profiles relative to a reference spectrum calculated for a homogeneous iron abundance of $A(\mathrm{Fe}) = 8.50$ over the entire star, in order to reveal the following profoundly worrisome fact: adopting the 'usual' approach to the modelling of spotted stars leads to errors in all four Stokes parameters. This is particularly well visible in Stokes I, resulting in spurious abundance estimates, but Stokes Q and V too turn out to be seriously affected, giving magnetic field estimates in error by more than 30 per cent! Looking for example just at the Stokes V signal, the 'usual' curve for a 4-kG field inside the spot is almost indistinguishable from the correct curve for a 3-kG field. Put it the other way round, one would considerably overestimate both magnetic field strength and abundance in the spot using the 'usual' incorrect mean model approach.

Our results clearly demonstrate that one cannot beat the limited resolution of a spectrograph by using Stokes Q and U profiles in order to obtain magnetic maps at ultrahigh resolution. It also becomes obvious that any reliable abundance and/or magnetic field estimates depend on the use of the correct atmospheric models for the spotted stellar surface. When these prerequisites of sufficient resolution and appropriate atmospheric models are not met, how then can one credibly establish secondary maxima or exceedingly small minima, in particular in places where the magnetic field strength drops from about 1 kG to a few hundred gauss?

8 MAPPING A SPOTTED STAR

The observed Stokes I profile of a rotating star is given by the integral over the properly Doppler-shifted local line and continuum intensities. A spot with enhanced abundances normally shows up as a bump, a dip or an asymmetry of the profile that varies with rotational phase. In Doppler mapping, this intensity information as a function of wavelength is used for the reconstruction of the surface abundance distribution, translating each wavelength difference (relative to the line centre) to a velocity swath on the stellar disc. As it turns out, this inversion is highly vulnerable to errors in the assumed atmospheric model.

To illustrate this point, we consider the profile differences presented in Fig. 4. The largest deviation in Stokes I is found near 4923.78 Å, about 9 km s^{-1} from the unshifted line position. This means that halfway from the disc centre to the limb, we get an estimate of the intensity which is incorrect by about 15 per cent when using the 'usual' model. In Stokes V, the errors can become even larger, up to 30 per cent for the dot–dashed red curve near 4923.65 Å. Of course such differences cannot be converted directly to abundance or field corrections in some region of the stellar surface because Doppler mapping involves global optimization involving a regularization function. Quite some time ago, Stift (1996) has pointed out that *'spurious abundances . . . constitute the sometimes entirely unphysical response of a particular regularization function to the spectral signature of the magnetic field'*, but it is clear that the same holds true for errors in the atmospheric structure of a spotted star.

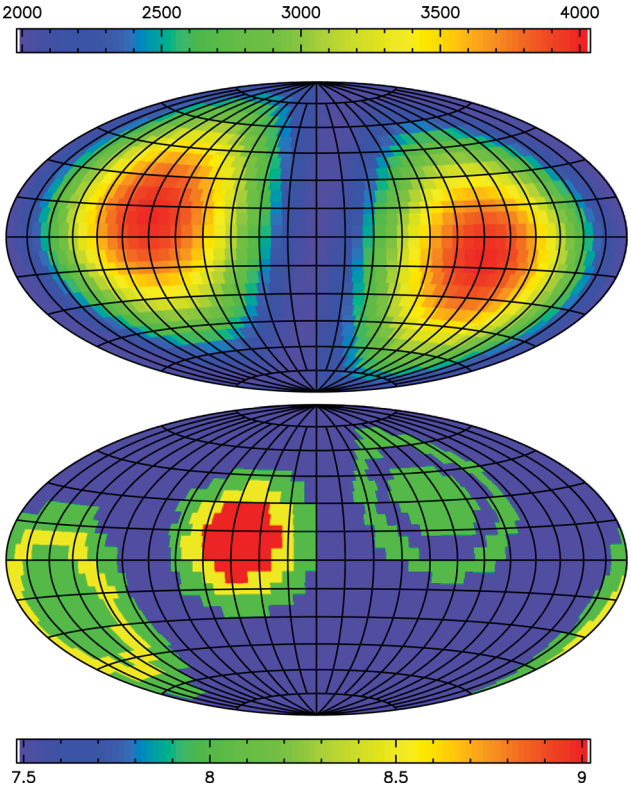

Figure 7. Iron abundance pattern (lower panel) and absolute field strength (upper panel) adopted for the modelling of phase-dependent Stokes spectra of a spotted star used in subsequent ZDM discussed in Section 8.

Let us demonstrate the validity of our argument with actual Doppler maps. Using the revived and refined Doppler mapping code of Stift (1996), we have inverted a series of Stokes I profiles corresponding in resolution, wavelength coverage and number of phases to the profiles used by K10. The star is inclined by 65° and covered by three spots as shown in Fig. 7; it rotates at $v\sin i = 18$ km s^{-1}, and the absolute strength of the dipolar magnetic field ranges from 2 to 4 kG. Inside the spots, the abundance can be as high as $A(\mathrm{Fe}) = 9.00$; outside the spots, it is $A(\mathrm{Fe}) = 7.50$. The 'usual' intensity profiles have been calculated with a $A(\mathrm{Fe}) = 8.00$ atmosphere, the correct profiles with the appropriate $A(\mathrm{Fe}) = 7.50, 8.00, 8.50$ and 9.00 atmospheres.

The inversion of a single line as in Kochukhov et al. (2004) leads to the results shown in Fig. 8. The lower panel shows an equal-area Hammer projection of the map obtained with the 'usual' profiles and the 'usual' Doppler mapping approach, namely under the assumption of a mean atmosphere inside and outside the spot, in this case a $A(\mathrm{Fe}) = 8.00$ atmosphere. In the upper panel, we have inverted the correct profiles in exactly the same 'usual' way. Both inversions result in a comparable quality of the fit to the input profiles, and both inversions display respective abundance maps that do not look unreasonable at all. It is obvious that the upper panel of Fig. 8 does not resemble the lower panel of Fig. 7, but we won't dwell here on the problem of finding the true extensions of spots, their contrast and number (for this, see e.g. Khokhlova 1976; Goncharskii et al. 1982). We rather want to concentrate on pointing out the mapping errors introduced by the differences between the metallicity assumed for the 'usual' inversion and the actual metallicities in the spotted star.

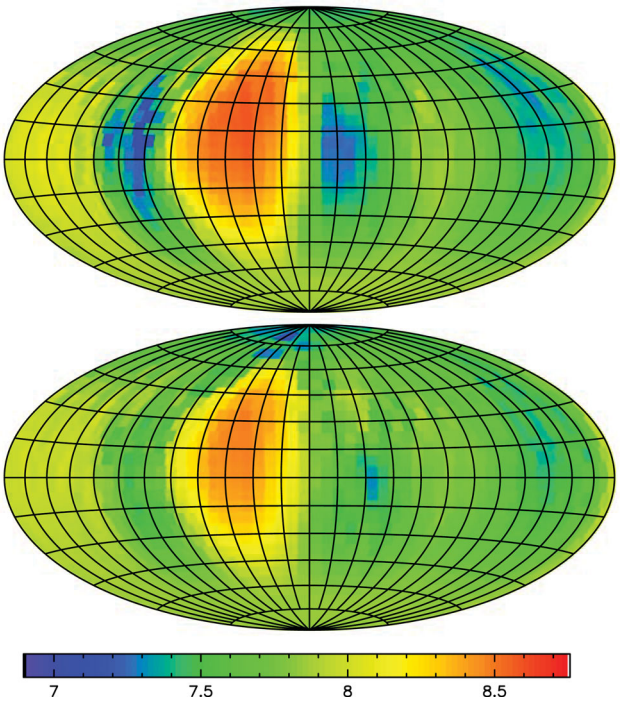

Figure 8. Hammer equal-area projection of abundance distributions derived by Doppler mapping from 20 phase-dependent synthetic Stokes *I* profiles of the Fe II line at 4923.927 Å. Synthetic profiles taken for input have been calculated for a star covered by three spots as shown in Fig. 7; the iron abundance is up to $A(\mathrm{Fe}) = 9.00$ in the spots and $A(\mathrm{Fe}) = 7.50$ in the remaining atmosphere. One set of profiles is based on the correct atmospheric models, the other set on the 'usual' approach with a mean model of $A(\mathrm{Fe}) = 8.00$. The latter is employed in both inversions which lead to the maps shown in the respective lower ('usual' profiles) and upper (correct profiles) panels.

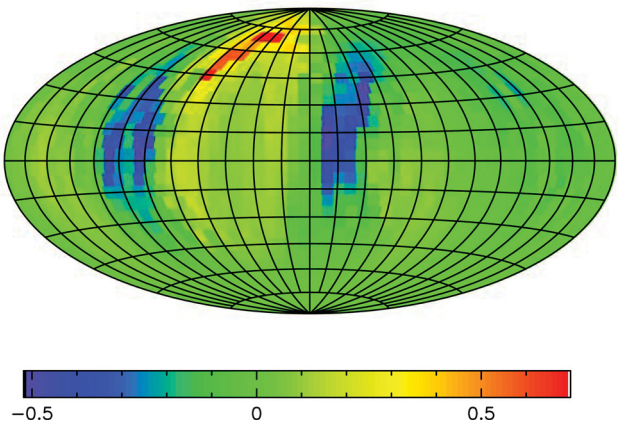

Figure 9. Same data as in Fig. 8 but displaying the difference (dex) between the respective abundance maps in the sense 'correct' minus 'usual' line spectrum.

Note the conspicuously different respective extensions of the main spot and the spurious structure showing up in several places.

To make it clear how serious the problem facing Doppler mapping really is, we plot the difference between the map obtained with the correct profiles and the 'usual' map. As revealed in Fig. 9, the differences between the respective abundances go from −0.5 dex to almost +0.7 dex, a remarkably large range given the relatively small error in the assumed abundance of the stellar atmosphere over most of the stellar surface. Note the spurious gradients near the borders of the actual strong spot.

9 CONCLUSIONS AND OUTLOOK

It is not easy to assess which of our findings will have the most sobering effect on (Zeeman) Doppler mapping enthusiasts keen on claiming to have found small-scale and high-contrast structure on the surfaces of magnetic Ap stars. What we would certainly consider most disturbing is the fact that despite the use of high S/N full Stokes *IQUV* spectra, ZDM with Tikhonov regularization as carried out for example by K02 and K10 can lead to abundance distributions and magnetic field maps that are demonstrably and unequivocally incorrect. This singularly strong statement is justified by the following considerations: the far-reaching claims by K10 are not based on tolerable approximations to the atmospheric structure of spotted stars since K10 not only neglect well-established physics of stellar atmospheres explored decades ago by Chandrasekhar (1935), but they also discard among others recent well-founded findings and recommendations made by Khan & Shulyak (2007). There can be no doubt that complex Zeeman Doppler maps with high-contrast abundance distributions and small-scale magnetic features can by no means be correct when local Stokes *I* profiles are in error by as much as 10 per cent of the continuum and when field estimates based on local Stokes *Q* and *V* profiles are in error by 30 per cent and more. The fate of the K10 paper is shared by a number of similar analyses (see e.g. Lüftinger et al. 2010). Having been made to believe that full Stokes profiles provide sufficient information to map not only 2D abundance and magnetic field distributions, but also 3D abundance stratifications (Lüftinger et al. 2008, but see Stift & Alecian 2009), it is discouraging that excellent ZDM codes like INVERS10 used by K10 can yield good fits to the observed Stokes *IQUV* profiles even when the adopted local line profiles are grossly in error. The results shown in Fig. 9 were equally surprising since they reveal that the adoption of an atmospheric model of mean metallicity in the Doppler mapping procedure – the respective correct models for the star and its spots differ by at most ±1.00 dex from this mean model – leads to local abundance discrepancies of between −0.50 and +0.70 dex. Considering the fact that at $A(\mathrm{Fe}) = 8.00$, metallicity effects are still relatively small and that they increase drastically for $A(\mathrm{Fe}) > 9.50$ (see Figs 1 and 2), we are not overly optimistic as, for example, to the reliability of the iron distribution derived by K10, where the adopted atmosphere with $A(\mathrm{Fe}) = 8.50$ differs from the 'local' atmospheres by as much as 2 dex.

Let us also dwell a bit on a previously unnoted, but not altogether surprising, complication that must be taken into account when applying ZDM. The adoption of a mean atmosphere for a spotted star will not only lead to erroneous surface abundance patterns, but also to incorrect magnetic geometries. In fact, it turns out that the Stokes *Q*, *U* and *V* profiles suffer considerably from metallicity-related effects; the adoption of a mean atmosphere for a spotted star can induce spurious changes of about 30 per cent and more in the maximum polarization signal. These wavelength- and phase-dependent profile changes will necessarily translate to errors in the distribution of magnetic field strength and direction. Given all the systematic errors in the four Stokes parameters which result from the use of a mean atmosphere, it could then prove premature to combine abundance and magnetic maps in an effort to verify how these data match theoretical predictions from the diffusion model (Michaud 1970) or to correlate the radial field and abundance distributions of various elements as done by K02.

Even less surprisingly, it is shown that the existence of 'small-scale magnetic structures' and of 'high-contrast magnetic spots' cannot at present be ascertained at any acceptable level of confidence. Even apparently moderate errors in the assumed atmosphere model can lead to non-negligible errors in the inferred magnetic field of a small, high-contrast spot. Any reliable detection of such a magnetic spot would only be possible with a much higher spectral resolution than available to K02 or K10, and it would require a fit to the Stokes Q, U and V profiles to at least 0.1–0.2 per cent. One should therefore consider magnetic fine structure as, for example, shown in fig. 7 of K10 to be largely an artefact of regularization.

In view of our results, the outlook for ZDM is a bit bleak but not hopeless. Success in the quest for more reliable maps of chemically peculiar stars depends on the ability to eschew the use of a mean atmosphere, replacing it with a whole grid of stellar atmospheres with different abundances of all the elements important enough to influence the temperature structure of the atmosphere (see again Khan & Shulyak 2007). As experience with CossamSpot shows this might put serious strain on computing resources, but there is no way around it. In return, abundance maps based on the correct atmosphere models might exhibit less spectacular amplitudes and the contrast might diminish, reducing the complexity of the computations. It is clear that ZDM is still in its infancy but multicore computer architectures in combination with modern object-oriented programming paradigms and powerful compilers will make it possible to enter the next phase. Keep, however, in mind that this approach is still full of (it is hoped) acceptable approximations and that more difficulties are lurking behind the bend: the influence of magnetic fields on the atmospheric structure, stratification, 2D and 3D stellar atmospheres for latitude- and longitude-dependent stratifications, etc.

ACKNOWLEDGMENTS

Thanks go to AdaCore for providing the GNAT GPL Edition of its Ada2005 compiler. Comments by the referee, Professor J. Landstreet, have helped to clarify issues and have resulted in an improved presentation of the results.

REFERENCES

Alecian G., Stift M. J., 2004, A&A, 416, 703
Alecian G., Stift M. J., 2007, A&A, 475, 659
Alecian G., Stift M. J., 2010, A&A, 516, A53
Asplund M., Grevesse N., Sauval A. J., Scott P., 2009, ARA&A, 47, 481
Auer L. H., Heasley J. N., House L. L., 1977, ApJ, 216, 531
Baschek B., Holweger H., Traving G., 1966, Abhandlungen Hamburger Sternwarte, 8, 26
Bischof K. M., 2005, Mem. Soc. Astron. Ital. Suppl., 8, 64
Brown S. F., Donati J.-F., Rees D. E., Semel M., 1991, A&A, 250, 463
Chandrasekhar S., 1935, MNRAS, 96, 21
Chmielewski Y., 1979, Publ. Obs. Genève, Série B, Fasc. 7, Spectres Stellaires Synthétiques: Programmes de Calcul. L'Observatoire de Genève, Genève
Cowley C. R., Hubrig S., Ryabchikova T. A., Mathys G., Piskunov N., Mittermayer P., 2001, A&A, 367, 939
Goncharskii A. V., Stepanov V. V., Khokhlova V. L., Yagola A. G., 1982, SvA, 26, 690
Gonzalez J.-F., Artru M.-C., Michaud G., 1995, A&A, 302, 788
Hubeny I., Lanz T., 1995, ApJ, 439, 875
Hubeny I., Hummer D. G., Lanz T., 1994, A&A, 282, 151
Hui A. K., Armstrong B. H., Wray A. A., 1978, J. Quant. Spectrosc. Radiative Transfer, 19, 509
Khan S. A., Shulyak D. V., 2007, A&A, 469, 1083
Khokhlova V. L., 1976, SvA, 19, 576
Kochukhov O., Wade G. A., 2010, A&A, 513, A13 (K10)
Kochukhov O., Piskunov N., Ilyin I., Ilyina S., Tuominen I., 2002, A&A, 389, 420 (K02)
Kochukhov O., Drake N. A., Piskunov N., de la Reza R., 2004, A&A, 424, 935
Kupka F., Piskunov N., Ryabchikova T. A., Stempels H. C., Weiss W. W., 1999, A&AS, 138, 119
Kurucz R. L., 2005, Mem. Soc. Astron. Ital. Suppl., 8, 14
Kurucz R., Bell B., 1995, Kurucz CD-Rom No. 23
Kuschnig R., Wade G. A., Hill G. M., Piskunov N., 1998, Contr. Astron. Obser. Skalnate Pleso, 27, 470
LeBlanc F., Monin D., Hui-Bon-Hoa A., Hauschildt P. H., 2009, A&A, 495, 937
Leone F., Manfré M., 1997, A&A, 320, 257
Lüftinger T., Kuschnig R., Weiss W. W., 1998, Contr. Astron. Obser. Skalnate Pleso, 27, 473
Lüftinger T., Kuschnig R., Piskunov N. E., Weiss W. W., 2003, A&A, 406, 1033
Lüftinger T., Kochukhov O., Ryabchikova T., Piskunov N., Weiss W. W., Ilyin I., 2008, Contr. Astron. Obser. Skalnate Pleso, 38, 335
Lüftinger T. et al., 2010, A&A, 509, A43
Maitzen H. M., 1976, A&A, 51, 223
Michaud G., 1970, ApJ, 160, 641
Mihalas D., 1970, Stellar Atmospheres. Freeman & Co., San Francisco
Peytremann E., Baschek B., Holweger H., Traving G., 1967, Rapport Interne, Obs. Genève
Piskunov N. E., Kupka F., Ryabchikova T. A., Weiss W. W., Jeffery C. S., 1995, A&AS, 112, 525
Piskunov N., Stempels H. C., Ryabchikova T. A., Malanushenko V., Savanov I., 1998, Contr. Astron. Obser. Skalnate Pleso, 27, 482
Rees D. E., Durrant C. J., Murphy G. A., 1989, ApJ, 339, 1093
Rice J. B., Wehlau W. H., Khokhlova V. L., 1989, A&A, 208, 179
Stift M. J., 1985, MNRAS, 217, 55
Stift M. J., 1996, in Strassmeier G., Linsky J. L., eds, Proc. IAU Symp. 176, Stellar Surface Structure. Kluwer, Dordrecht, p. 61
Stift M. J., 1998, in Asplund L., ed., Proc. Lecture Notes in Computer Science, Vol. 1411, Reliable Software Technologies – Ada Europe '98. Springer, Heidelberg, p. 128
Stift M. J., 2000, Peculiar Newslett., 33, 27
Stift M. J., Alecian G., 2009, MNRAS, 394, 1503
Stift M. J., Dubois P. F., 1998, Comput. Phys., 12, 150
Stift M. J., Leone F., 2003, A&A, 398, 411
Strom S. E., Kurucz R., 1966, AJ, 71, 181
Vogt S. S., Penrod G. D., Hatzes A. P., 1987, ApJ, 321, 496
Wade G. A., Bagnulo S., Kochukhov O., Landstreet J. D., Piskunov N., Stift M. J., 2001, A&A, 374, 265

This paper has been typeset from a TEX/LATEX file prepared by the author.